RED: RFID-Based Eccentricity Detection for High-Speed Rotating Machinery

Yuan He, *Senior Member, IEEE*, Yilun Zheng, *Student Member, IEEE*, Meng Jin, *Student Member, IEEE*, Songzhen Yang, *Student Member, IEEE*, Xiaolong Zheng, *Member, IEEE*, and Yunhao Liu, *Fellow, IEEE*

Abstract—Eccentricity detection is a crucial issue for high-speed rotating machinery, which concerns the stability and safety of the machinery. Conventional techniques in industry for eccentricity detection are mainly based on measuring certain physical indicators, which are costly and hard to deploy. In this paper, we propose RED, a non-intrusive, low-cost, and real-time RFID-based eccentricity detection approach. Differing from the existing RFID-based sensing approaches, RED utilizes the temporal and phase distributions of tag readings as effective features for eccentricity detection. RED includes a Markov chain based model called RUM, which only needs a few sample readings from the tag to make a highly accurate and precise judgement. The design of RED further addresses practical issues, such as parameterizing the RUM model, making it robust to dynamic and noisy environments, and considering how the doppler shift may affect our system. We implement RED with COTS RFID reader and tags, and evaluate its performance across various scenarios. The overall accuracy is 93.6 percent and the detection latency is 0.68 seconds in average.

Index Terms—RFID, eccentricity detection, high-speed, sensing

1 Introduction

Rotating machinery is a widely used part in industrial equipments, ranging from small motor to massive generator as shown in Fig. 1. Rotating machinery on those equipments generally plays a key function and counts the major portion of the manufactory cost. It's therefore necessary and crucial to ensure the mechanical health and normal operation of the rotating machinery. When a rotor is rotating, it keeps producing a centrifugal force. When the rotating speed goes high, the resulting strong centrifugal force can make a rotor's center axis deviate from its initial position, as shown in Fig. 2. This is so-called eccentricity. Eccentricity is generally harmful to rotating machinery. Countless industrial accidents and losses are caused by the eccentricity of rotating machinery [1]. Eccentricity detection, namely to detect eccentricity within specified time, becomes an indispensable component of rotating machinery in modern industry.

Conventional techniques in industry for eccentricity detection [2], [3], [4], [5], [6], [7] are mainly based on measuring certain physical indicators, such as electrical current, sound, temperature, vibration, etc. The vibration measurement is the most widely used approach to monitor the health of machinery but existing techniques that can directly measure the vibration usually require embedding special sensors and data acquisition instruments with considerable costs [8]. For the small rotating machinery, it is even impossible to embed extra hardware when they are manufactured. Hence in typical industrial scenarios, those small-size and cheap rotating machines are checked periodically by handheld detectors [9] and the detection latency will be hours or even days. To avoid catastrophic accidents, it is necessary and significant to detect faults early before the severe failure stage of the machinery [10], so many researchers are committed to developing time-efficient detection systems. The typical detection latency is desired at the level of second [11]. The above facts call for a low-cost, non-intrusive, real-time technique for eccentricity detection on the ordinary cheap rotating machinery.

Recent advances in Radio Frequency IDentification (RFID) make it a promising technique for sensing physical phenomenon. The existing works have explored RFID-based sensing in varied cases, e.g., orientation detection [12], [13], [14], [15], humidity sensing [16], vibration inspection [17] , motion detection [18] and touch sensing [19]. Successes in those cases demonstrate advantages of RFID-based sensing, especially the low cost and ease of deployment. Then an open problem naturally comes to our mind: Can RFID-based sensing detect eccentricity? After careful thinking and all-sided analysis, we find this problem is extremely challenging, due to the following reasons.

- *High-speed rotation produces discrete tag readings*. The rotation speed of rotating machinery is very high, typically over thousands RPM (revolutions per

- *Y. He, Y. Zheng, M. Jin, and S. Yang are with the School of Software and BNRist, Tsinghua University, Beijing 100084, China. E-mail: he@greenorbs.com, zhengyl15@tsinghua.org.cn, mengj@mail.tsinghua.edu.cn, yangsz14@163.com.*
- *X. Zheng is with the School of Software and Beijing Key Lab of Intelligent Telecommunication Software and Multimedia, Beijing University of Posts and Telecommunications, Beijing 100876, China. E-mail: zhengxiaolong.zxl@gmail.com.*
- *Y. Liu is with the Department of Computer Science and Engineering, Michigan State University, East Lansing, MI 48824 USA. E-mail: yunhao@greenorbs.com.*

Manuscript received 20 July 2018; revised 2 Dec. 2019; accepted 10 Dec. 2019. Date of publication 27 Dec. 2019; date of current version 4 Mar. 2021. (Corresponding author: Yuan He.) Digital Object Identifier no. 10.1109/TMC.2019.2962770

Fig. 1. Some applications of rotating machineries, which are power generator, motor, car engine, and pump.

minute). The sampling frequency of commercial RFID tags is around 40Hz. When we attach an RFID tag to the surface of the rotor and let them rotate together, the RFID reader can only get sub-Nyquist sampling. The tag readings are essentially discrete and correspond to scattered positions of the tag.

- *High precision requirement*. According to practice in industry, the eccentricity cannot exceed a specified distance, which is generally several millimeters or even shorter. Note that the readings from RFID tags are dynamic and noisy, while the resolution of received signal strength indicator (RSSI) readings is only 0.5 dB [20]. It is therefore infeasible to identify eccentricity, solely based on the RSSI and phase readings.
- *Real-time requirement*. Due to the high-speed rotation, eccentricity that exceeds a predefined threshold must be detected in real time. Otherwise, accidents are likely to happen before one can take any countermeasure.
- *High reliability requirement*. Not only false negative but also false positive alarms should be avoided in eccentricity detection. Excessive false positives will cause unnecessary downtime of the machinery, which is also a kind of loss.

In this paper, we propose RED, an RFID-based approach tailored for eccentricity detection in high-speed rotating machinery. The hardware requirement of RED is very simple: an RFID tag attached to the surface of the rotor and an RFID reader deployed nearby. The tag rotates with the rotor at the same speed, returning readings periodically to the reader. The design of RED is based on the following insight: Despite that every single reading is disorganized, the distribution of readings is stable if there is no eccentricity. When the rotor's eccentricity increases, the distribution of readings will also change. How much the distribution is varied reflects the distance of eccentricity (i.e., shift). We address non-trivial challenges in implementing the above idea and make RED a universal, non-intrusive, and low-cost solution. The contributions of this work are summarized as follows.

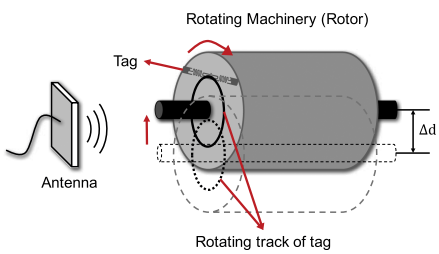

Fig. 2. A sketch of static eccentricity.

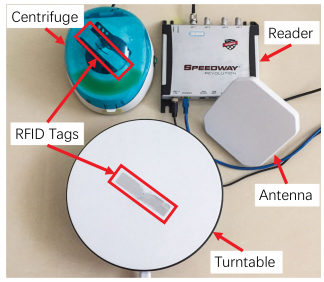

Fig. 3. Experiment setup.

- In the context of high-speed rotation, we disclose the relationship between eccentricity and the probabilistic distribution of RFID readings. Instead of judging according to the RSSI and phase values, we identify the temporal and phase distributions of signals as effective features for eccentricity detection.
- We propose a Markov chain based model called RUM for eccentricity detection. With the RUM model, RED only needs a few sample readings from the tag to make a highly accurate and precise judgement. We further address practical issues, such as parameterizing the Rum model, making it robust to dynamic and noisy environments, and considering how the doppler shift may affect our system.
- As a non-intrusive approach, RED is applicable to all kinds of rotating machinery. We implement RED with commercial-of-the-shelf RFID reader and tags, and evaluate its performance across various scenarios. The overall accuracy is 93.6 percent and the detection latency is 0.68 seconds in average.

The rest of this paper is organized as follows. In Section 2, we describe our empirical studies. The design details of model RUM and the overview of RED are presented in Section 3. Discussions about practical factors are in Section 4. Implementation and evaluation are described in Section 5. Section 6 discusses related works. We conclude and discuss future work in Section 7.

2 Empirical Study

Generally speaking, there are two types of eccentricity, namely *static* eccentricity and *dynamic* eccentricity [21]. In the static case, the rotation axis is the center of the rotor but the it has a shift from the center of the stator. In the dynamic case, the rotor also has a shift but the rotation axis remains as the center of the stator. In this paper we mainly focus on the static eccentricity and the dynamic case is discussed in Section 4.5. Fig. 2 shows a static eccentricity sketch. When eccentricity happens, the axis of the rotor has a shift Δd relative to the initial position.

Fig. 3 shows the devices that conduct the experiments. We use a centrifuge and a turntable. Their rotation speeds are 10,000 RPM and 1 RPM, respectively. We simulate the eccentricity by moving the whole device away from the antenna. Alien UHF passive RFID tags [22] are attached onto the surface of these two devices. An ImpinJ Speedway

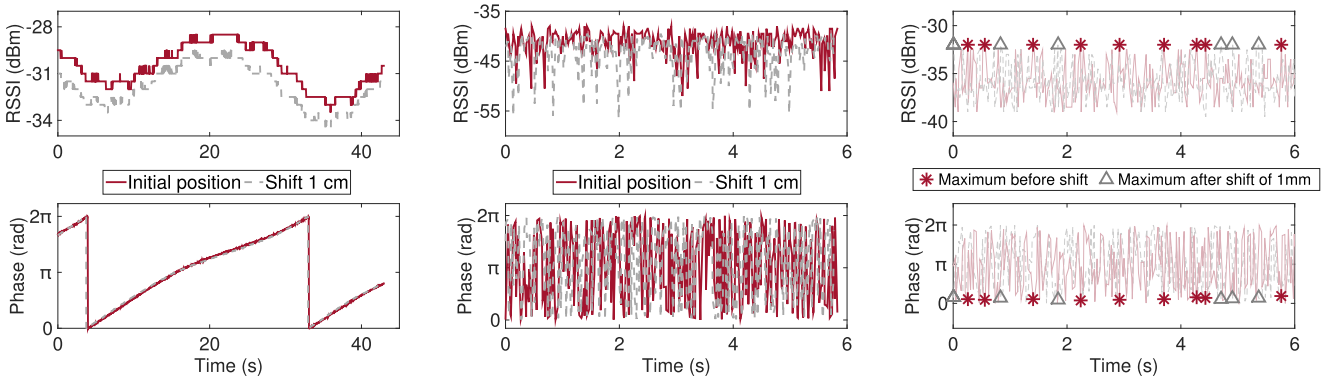

(a) Tag rotates at 1 RPM (b) Tag rotates at 10000 RPM (c) The maximums of RSSI and their corresponding phase values before and after eccentricity

Fig. 4. Measured RSSI and phase before and after the eccentricity (shifting away from the antenna).

R420 RFID reader [20] and a Laird circular polarized antenna are nearby, receiving the signals backscattered by the tags. From each sampling, the reader gets a RSSI and a phase value.

When the tag rotates at 1 RPM, the signal changes periodically as Fig. 4a shows. In a period, RSSI fluctuates within a stable interval, increasing from the minimum to the maximum and then decreasing. At the same time, the phase monotonically increases from 0 to 2π. We also find that when the tag rotates for half a circle, the RSSI and phase readings change for a period due to polarization [23].

Fig. 4b shows the received signals when the tag rotates at 10,000 RPM. Different from Fig. 4a, the signal is highly dynamic and discrete because of the high rotation speed and sub-Nyquist sampling. But we can still observe some difference caused by the shift of 1 cm. When the distance between the tag and the antenna increases, the maximum and the minimum values of the RSSI become smaller. Unfortunately, the phase readings are indistinguishable.

We can observe from Fig. 4c that when the distance increases, the number of maximum decreases during a certain time period. That is, the expected time interval between two maximum increases. The corresponding phase values concentrate close to a certain value. The reason is that the periods of RSSI and phase are same, so the corresponding phase value of every RSSI is fixed if the environment remains the same. Considering the dynamics in RSSI readings, we regard the RSSI readings that are above a certain threshold as the maximum values, and define the corresponding sample as *E-points*. The RSSI threshold is based on a pre-defined percentage value (e.g., points in the upper 5 percent of the RSSI range are regarded as E-points). When the threshold has been set in the initialization, it is a fixed value and does not change any more. Every time we get an E-point, we compute the time interval (denoted by Int) between this and the last E-point. We also compute the phase difference (denoted by $Diff$) between this and the last E-point. If the distance between the antenna and the tag increases, the expected Int increases while the expected $Diff$ decreases.

2.1 Signal Analysis and Feature Extraction

According to the above findings, an intuitive idea for eccentricity detection is to detect whether the maximum of RSSI has changed. Considering the RSSI reading fluctuations, we can hardly identify the maximum value, unless a sufficiently large number of samples are collected. What's more, the resolution of RSSI is 0.5 dB due to hardware limitation. When the shift is small, such as 1 mm, the maximum of RSSI stays constant as Fig. 4c shows. So it doesn't work if we only focus on the RSSI value of maximum.

2.2 The Stability of The Two Features

We repeat the experiments several times, in different conditions to observe the distribution of phase difference and time interval of E-points. From Fig. 5 we can see that these two features are stable, when the tag stays at a fixed position. The CDFs of the two features are almost same over four hours. Fig. 8 shows the stability of the RSSI and phase measurements of a static tag and a reader for 10 minutes to define the baseline of fluctuations. We also repeat the experiments with two different tag (Tag 1 and Tag 2) of same type that located

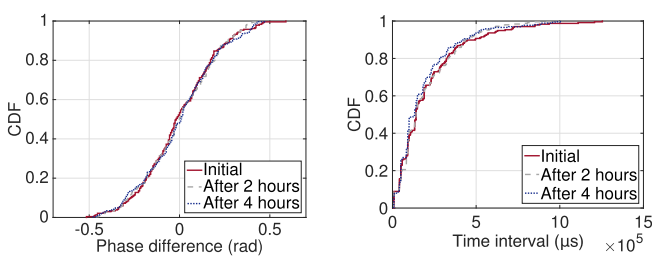

(a) The CDF of phase difference (b) The CDF of time interval

Fig. 5. The CDF of phase difference and time interval over four hours.

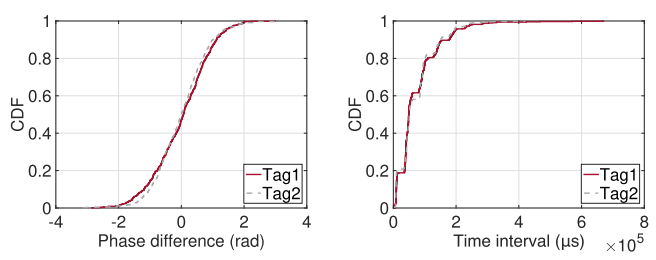

(a) The CDF of phase difference (b) The CDF of time interval

Fig. 6. The CDF of phase difference and time interval of different tags.

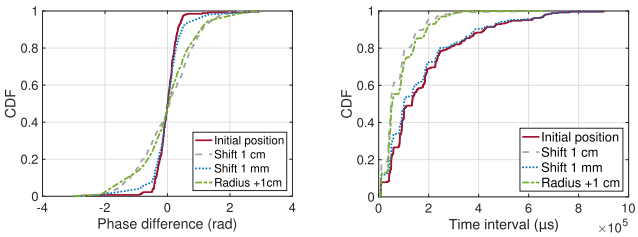

(a) The CDF of phase difference (b) The CDF of time interval

Fig. 7. The CDF of phase difference and time interval before and after the shift (shifting towards the antenna).

at the same position. Fig. 6 shows that the distributions of phase difference and time interval are almost same. The hardware differences among individuals will not influence the effectiveness of our design, so we can replace tags in the practical situation.

2.3 The Distinguishability of The Two Features

Finally we compare the distribution of the two features before and after eccentricity. From Fig. 7 we can see that the result is consistent with our analysis. When the tag approaches the antenna, the maximum and the minimum of RSSI increases, and the number of E-points increases. As a result, the range of phase difference increases and the range of time interval decreases.

2.4 Findings and Analysis

Then we will explain why eccentricity can affect Int and $Diff$. Consider the scenario where the tag approaching the antenna, E-points are selected when their RSSI readings are above a certain threshold. Therefore, not only those points having really maximum RSSI, but also the points close to the maximum points are likely to be regarded as E-points. We call those points are in the neighborhood of maximum points. Before the shifting, the neighborhood interval is small so the E-points have more similar phase values. When the tag approaches the antenna, all points RSSI increase and E-points will get denser so Int decreases. The internal change is that the neighborhood is extended and becomes wider while the pre-defined threshold is a constant. Since the E-points appear in a wider area, the range of their phase difference ($Diff$) increases. Based on these findings and analysis, we can design an RFID-based eccentricity detection system.

3 RED in Principle

Our findings are based on the statistical regularities of the accumulation of data, which is difficult to get in very short time. Besides, we can't get the training data under the environment of eccentricity in a real scenario, so we have no idea about how the distribution is after eccentricity when we deploy the devices in a new environment.

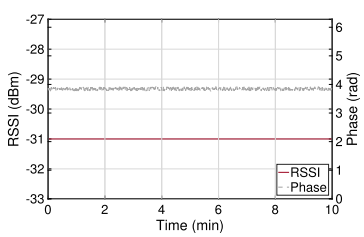

Fig. 8. The stability of the RSSI and phase measurements.

TABLE 1
Some Typical Symbols in RED

Symbol	Meaning
T_i	Arriving time of the E-point E_i
Ph_i	Phase of the E-point E_i
w	The length of the observation window
$P^{unecc}_{trans}(S_i\|S_{i-1})$	The transition probability between two sequential states in the non-eccentricity scenario
$P^{ecc}_{trans}(S_i\|S_{i-1})$	The transition probability between two sequential states in the eccentricity scenario
$P^{unecc}_{out}(Int_i, Diff_i)$	The probability that we can get an observation $(Int_i, Diff_i)$ when the eccentricity has not occurred
$P^{ecc}_{out}(Int_i, Diff_i)$	The probability that we can get an observation $(Int_i, Diff_i)$ when the eccentricity occurred
$P(ecc)$	The prior probability which captures the occurrence frequency of eccentricity
$P(Int_i, Diff_i)$	The probability of the observation $(Int_i, Diff_i)$
λ	The mean value of Int
Sa	The mean value of the sampling interval
R_E	The RSSI range of the E-points
R_{RSSI}	The value range of all the observed RSSIs
P_{unecc}	The probability that the eccentricity has not occurred
P_{ecc}	The probability that the eccentricity has occurred

In this section, we first describe an overview of the eccentricity detection model, named RUM, which is used to meet the real-time requirement, followed by detailed discussion of its main components including estimating the distribution after eccentricity. At last, we describe how RED work as a whole system. The symbols used in this paper are listed in Table 1.

3.1 RUM: A Model for Eccentricity Detection

Although the shift caused by eccentricity dose cause change in distance between the antenna and the tag, and in turn causes changes in RSSI and phase, the changes is too small to detect so relying on the absolute values of RSSI and phase is not a good idea. However, the statistical property of RSSI and phase indeed reflects the impact of eccentricity as shown in our experiment results and analysis before. So we choose to design a Markov chain based model, using $Diff$ and Int as input. Specifically, the problem of eccentricity detection can be stated as: given a sequence of E-point measurements, what is the probability that the center of the rotating machinery has deviated from its initial position?

Given the length of the observation window w, we can get a E-point sequence $E_i = \{(T_i, Ph_i)|n-w \le i \le n-1\}$. Then we can get the time interval sequence as $Int_i = \{T_{i+1} - T_i|n-w \le i \le n-2\}$, and the phase difference sequence as $Diff_i = \{Ph_{i+1} - Ph_i|n-w \le i \le n-2\}$. Now the problem is how to instantly detect the change in the Int and $Diff$ sequences which indicates the eccentricity.

In this model, we mainly focus on two probabilities. The probability that every observation $(Int_i, Diff_i)$ occur is one indicator of eccentricity we use, denoted by $P^{unecc}_{out}(Int_i, Diff_i)$, because it change as the distributions change caused by eccentricity. In addition to the probabilities of occurrence,

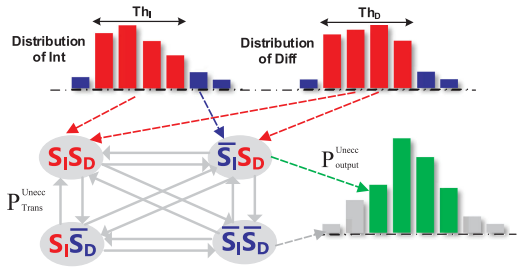

Fig. 9. Illustration of the RUM model.

the transition probabilities between two observation is another key indicator.

To compute the transition probabilities conveniently, in the RUM model, we define four states, i.e., States S_IS_D, $\overline{S_I}S_D$, $S_I\overline{S_D}$, and $\overline{S_I}\overline{S_D}$ (as shown in Fig. 9), to describe how likely the observed $(Int_i, Diff_i)$ implies a non-eccentricity. Specifically, given the distributions of Int and $Diff$ when eccentricity has not occurred, if both the observed Int_i and $Diff_i$ locate within the pre-defined confidence intervals of Int and $Diff$ (denoted by Th_I and Th_D), we identify that $(Int_i, Diff_i) \in S_IS_D$. State $\overline{S_I}$ (or $\overline{S_D}$) means that the observed Int_i (or $Diff_i$) falls outside the confidence interval Th_I (or Th_D). Th_I and Th_D are not thresholds. They are both values of percentage to denote an interval in the distribution of Int or $Diff$. They are not fixed and should be calculated in the initialization phase of the system. The system collects enough samplings to get the distribution of Int and $Diff$, and then determines the central interval which can cover most of the samplings (95 percent). We assume that under normal conditions, samples will appear in this interval. Otherwise, likely there is an eccentricity. Therefore, they can be used to characterize the state transition probability.

Now the sequence of $(Int_i, Diff_i)$ can be translated to a sequence of states $\mathbf{S_n} = \{S_{n-1}, \ldots, S_{n-w}\}$. Theoretically, if the eccentricity has not occurred, the observed $(Int_i, Diff_i)$ are likely to stay on State S_IS_D. However, due to the noises and interferences, the observed $(Int_i, Diff_i)$ may occasionally transfer to States $\overline{S_I}S_D$, $S_I\overline{S_D}$, or even $\overline{S_I}\overline{S_D}$, but the transition probabilities are low. If eccentricity happens, the transition probabilities may increase. As a result, we can compute how likely the transitions happen in every observation window as an indicator of eccentricity.

Specifically, the probability that we can observe a transition chain $\{S_{n-1}, \ldots, S_{n-w}\}$ under the non-eccentricity scenario is

$$P_{chain}^{unecc} = \prod_{\text{i=n-w}}^{n} P_{trans}^{unecc}(S_i|S_{i-1}). \tag{1}$$

Then we can evaluate how likely we observe a state sequence $\mathbf{S_n}$ under the non-eccentricity scenario using a normalized metric *PoC* as follow:

$$PoC^{unecc}(\mathbf{S_n}) = max\left\{\frac{P_{chain}^{unecc} - \min_{s\in S}(P_s)}{\max_{s\in S}(P_s) - \min_{s\in S}(P_s)}, 1 - \frac{rank(P_{chain}^{unecc}) - 1}{|S|}\right\}, \tag{2}$$

where $\mathbf{S}$ is the set of all the possible state sequences that include n motions. $rank(P_{chain}^{unecc})$ is the ranking of P_{chain}^{unecc} among all the P_s ($s \in \mathbf{S}$).

Based on the P_{out}^{unecc} of each observed $(Int_i, Diff_i)$ and the estimated $PoC^{unecc}(\mathbf{S_n})$ for the state sequence $\mathbf{S_n}$, we can give a normalized metric $P^{unecc}(\mathbf{S_n})$ to describe how likely that the eccentricity does not occur

$$P^{unecc}(\mathbf{S_n}) = PoC^{unecc}(\mathbf{S_n}) \cdot min\{P_{out}^{unecc}(Int_{n-1}, Diff_{n-1}), \ldots, P_{out}^{unecc}(Int_{n-w}, Diff_{n-w})\}. \tag{3}$$

Similarly, we can also get a normalized metric $P^{ecc}(\mathbf{S_n})$ to describe how likely the state sequence $\mathbf{S_n}$ implies an eccentricity scenario. Once RED detects a state sequence which results in $P^{ecc}(\mathbf{S_n}) > P^{unecc}(\mathbf{S_n})$, it considers that an eccentricity occurs.

In the following subsections, we will discuss how to estimate P_{out} and PoC in detail.

3.2 P_{out} Estimation

The P_{out} estimation component aims to calculate the P_{out}^{unecc} and P_{out}^{ecc} for each observed $(Int_i, Diff_i)$ as an indicator of eccentricity. According to the Bayes theorem, we can calculate these two probabilities using the corresponding postetior probability of each observation $(Int_i, Diff_i)$, given the eccentricity has occurred or not, i.e., $P(Int_i, Diff_i|ecc)$ and $P(Int_i, Diff_i|unecc)$. The P_{out}^{unecc} and P_{out}^{ecc} can be formulated as

$$\begin{aligned} P_{out}^{unecc} &= \frac{(1-P(ecc))\cdot P(Int_i, Diff_i|unecc)}{P(Int_i, Diff_i)} \\ P_{out}^{ecc} &= \frac{P(ecc)\cdot P(Int_i, Diff_i|ecc)}{P(Int_i, Diff_i)}. \end{aligned} \tag{4}$$

Since $P(Int_i, Diff_i)$ is the same for eccentricity and non-eccentricity scenarios, we are only interested in calculating $P(Int_i, Diff_i|ecc)$, $P(Int_i, Diff_i|unecc)$, and $P(ecc)$

$$\begin{aligned} P_{out}^{unecc} &\propto (1 - P(ecc)) \cdot P(Int_i, Diff_i|unecc) \\ &\approx (1 - P(ecc)) \cdot P(Int_i|unecc) \cdot P(Diff_i|unecc) \\ P_{out}^{ecc} &\propto P(ecc) \cdot P(Int_i, Diff_i|ecc) \\ &\approx P(ecc) \cdot P(Int_i|ecc) \cdot P(Diff_i|ecc). \end{aligned} \tag{5}$$

It is difficult to give the accurate value of $P(Int_i, Diff_i|ecc)$ or $P(Int_i, Diff_i|unecc)$ directly due to the impact of uncertain factors like rotating speed and shifting distance. In order to obtain a feasible mathematical model, we have to consider them as random factors and assume that the probability division only causes negligible error. $P(ecc)$ can be obtained from the statistic data. Therefore, the key goal translates to obtaining $P(Int_i|unecc)$, $P(Diff_i|unecc)$, $P(Int_i|ecc)$, and $P(Diff_i|ecc)$. It seems that we can obtain these posterior probabilities just based on training samples of Int and $Diff$. However, in real world deployment of RED, Int and $Diff$ samples are all from the non-eccentricity scenario, making it difficult to obtain the empirical values of $P(Int_i|ecc)$ and $P(Diff_i|ecc)$.

Fortunately, the distributions of Int and $Diff$ are indeed highly related to the factors like the value range of the measured RSSIs and phases. If we can find an accurate model to

describe the relationship between these factors and the distribution of Int and $Diff$, then we can estimate the posterior probabilities without relying on the training phase. In the following, we focus on how to estimate $P(Int_i|unecc)$ and $P(Diff_i|unecc)$, which can be generalized to the estimation of $P(Int_i|ecc)$ and $P(Diff_i|ecc)$.

Estimation of $\mathbf{P(Int_i|unecc)}$. Consider that the sampling interval is random in RFID systems, $P(Int_i|unecc)$ is mainly determined by the occurrence probability of E-points P_E^{unecc} and P_E^{ecc}. Int follows the exponential distribution[1] as $Int \sim E(\lambda)$. Thus we have

$$P(Int_i|unecc) = \lambda e^{-\lambda Int_i}, \tag{6}$$

where $\lambda = \frac{Sa}{P_E^{unecc}}$, and Sa can be obtained from the specification of the RFID system. We will introduce how to estimate P_E^{unecc} and P_E^{ecc} in Section 3.3.

Estimation of $\mathbf{P(Diff_i|unecc)}$. The distribution of $Diff$ is highly determined by the phase range of the E-points $[\alpha, \beta]$. Therefore, considering that the sampling interval is random (as discussed earlier), $Diff$ (ranges from 0 to $\beta - \alpha$) will follow the uniform distribution as $Diff \sim U(\frac{\beta-\alpha}{2}, \frac{(\beta-\alpha)^2}{12})$. That is to say, theoretically we have

$$P(Diff_i|unecc) = \frac{1}{\beta - \alpha}. \tag{7}$$

However, environmental factors like noise and interference may affect the measurement of the phases. Therefore, assume that the measured value of the phase difference is $\widehat{Diff}_i$, then we have $\widehat{Diff}_i = Diff_i + w$, where w is the measurement noise which follows the normal distribution as $\delta_w \sim N(0, \sigma_w)$. Thus the measured $Diff$ follows the joint distribution of both uniform distribution and normal distribution, which can be estimated as follows:

$$P(Int_i|unecc) = \frac{1}{\beta - \alpha} \cdot \left[\Phi\left(\frac{Diff + \beta - \alpha}{\sqrt{2}\sigma_w}\right) - \Phi\left(\frac{Diff}{\sqrt{2}\sigma_w}\right)\right], \tag{8}$$

where $\Phi(\bullet)$ is the probability density function of the standard normal distribution. In practice, the value of α and β can be estimated based on the RSSI range of the E-points, which we will show in Section 3.3.

3.3 Estimation of P_E^{unecc} and P_E^{ecc}

As $P_E^{unecc} = \frac{R_E}{R_{RSSI}}$, we should estimate the range of the RSSIs and the phases of the E-points.

RSSI Range. As discussed in Section 3.2, $P(Int_i|unecc)$ is highly related to the proportion of the E-points (i.e., $P_E = \frac{R_E}{R_{RSSI}}$), which is further determined by the RSSI range of the E-Points (R_E) and the value range of all the sampled RSSIs (R_{RSSI}). Here, R_E is determined by the predefined threshold Th_p. Therefore, to estimate P_E, we have to estimate R_{RSSI}. In real world deployment of RED, the RSSI range in the non-eccentricity scenario can be estimated based on the RSSI samples. The RSSI range in the eccentricity scenario, however, needs to be estimated based on i) the RSSI range that in the non-eccentricity scenario (R_{RSSI}^{unecc}); and ii) the expected minimum shift distance can be detected by RED (namely Δd mentioned in Section 2). Specifically, assume that the effect of the polarization is negligible (since that the displacement of the tag is only in mm level), the RSSI range in the eccentricity scenario will change linearly compared with that in the non-eccentricity scenario. Therefore, if the rotating machinery shifts Δd, the corresponding variation in RSSI (denoted by ΔR) can be estimated by the Friis transmission formula [24].

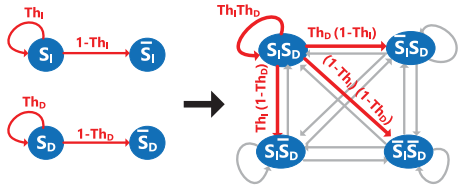

Fig. 10. Estimating of the transition probabilities.

Phase Range. Phase range of the E-points (i.e., $[\alpha, \beta]$) is an important information which can be used to estimate the distribution of $Diff$ in both eccentricity and non-eccentricity scenarios. In practice, the phase range can be estimated based on the proportion of the E-points P_E. Specifically, the experimental results in Section 2 shows that the relation between the RSSI and the corresponding phase can be regarded as a sine function. Thus given the proportion of the E-points under the non-eccentricity scenario (i.e., P_E^{unecc}), the value of α and β can be estimated by

$$\begin{aligned} \alpha &= \tfrac{\pi}{2} - arcsin\left[1 - 2 \cdot \left(\tfrac{\Delta}{R_E} + P_E^{unecc}\right)\right] \\ \beta &= \tfrac{\pi}{2} + arcsin\left[1 - 2 \cdot \left(\tfrac{\Delta}{R_E} + P_E^{unecc}\right)\right]. \end{aligned} \tag{9}$$

Note that we can get the phase range in the non-eccentricity scenario by setting $\Delta = 0$, while get the range in the eccentricity scenario by setting $\Delta = \Delta R$.

3.4 PoC Estimation

The main target of the PoC estimation component is to calculate the transition probability between each two states without relying on the training phase. In the following, we use the transition probabilities from State $S_I S_D$ to other states as a vehicle to explain the method to estimate the transition probabilities.

Assume that the transition between S_I and $\overline{S_I}$ and that between S_D and $\overline{S_D}$ are independent of one another. Based on this assumption, the transition probabilities between these "single states" (i.e., States S_I, $\overline{S_I}$, S_D, and $\overline{S_D}$) is solely determined by the confidence interval of the distributions of Int or $Diff$. For example, the probability of the transition from S_I to $\overline{S_I}$ can be simply calculated as $1 - Th_I$ and that of the transition from S_I to S_I is Th_I.

Then let's look at the transition probabilities between "combined states" ((i.e., States $S_I S_D$, $\overline{S_I} S_D$, $S_I \overline{S_D}$, and $\overline{S_I S_D}$). For example, the transition between $S_I S_D$ and $\overline{S_I} S_D$ can be considered as the result of two concurrent event: i) the transition between S_I and $\overline{S_I}$; and ii) the transition between S_D and S_D. Thus we have

1. Exponential distribution is the probability distribution that describes the time between events in a Poisson process, i.e., a process in which events occur continuously and independently at a constant average rate.

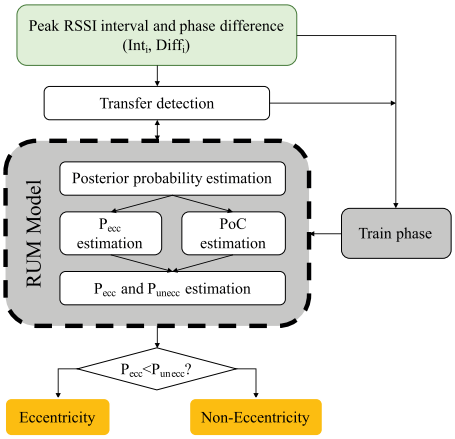

Fig. 11. The overview of RED.

$$P(\overline{S_I}S_D|S_IS_D) \approx P(\overline{S_I}|S_I) \cdot P(S_D|S_D) = (1 - Th_I) \cdot Th_D. \tag{10}$$

Similarly, we can get the transition probabilities between S_IS_D and States $S_I\overline{S_D}$, $\overline{S_I}S_D$, $\overline{S_I}\overline{S_D}$ as shown in Fig. 10.

3.5 Put it Together

Fig. 11 illustrates the key workflow of RED, which comprises a training phase and a eccentricity model (RUM).

Before RED start working, we have a short training phase. Through collecting the signals when the tag rotating with the machinery at original position for about 1 minute, we can get the original distribution of Int and $Diff$. These data are used in RUM not only as original probability, but also for estimating the distribution after eccentricity.

Then we can begin the process of eccentricity detection. First of all, the sampled raw signals from the tag are processed to extract the time interval between two peak RSSIs and the phase difference between their corresponding phases, i.e., Int and $Diff$. Then the data $(Int, Diff)$ acts as a input of RUM. According to the above content, RUM is able to continuously track the variation of Int and $Diff$, and instantly estimate the probabilities that the eccentricity has occurred or not, based on the distributions of Int and $Diff$ and how Int and $Diff$ change. At last, by comparing P_{unecc} and P_{ecc}, RED outputs the detection result.

4 RED in Practice

This section presents how we solve those problems our system may face in practice.

4.1 Fix Environment-Dependent Factors

The Friis transmission formula [24] is widely applied

$$P_R(d,\theta) = \frac{P_T G_{TR}^2 G_t^2 \lambda^4}{(4\pi)^4} \cdot \frac{X(\theta)^2}{d^4}, \tag{11}$$

where d is the distance between the tag and the antenna, θ is the polarization angle between the antenna and the tag, $P_R(r,\theta)$ is the power received at the reader, P_T is the power transmitted by the reader, G_{TR} is the gain of the reader transmitter/receiver antenna, G_t is the tag antenna gains,

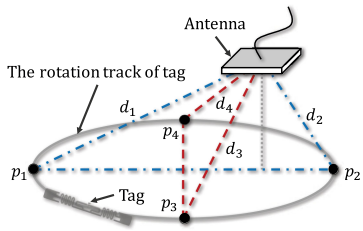

Fig. 12. The rotation track of tag.

and λ is the carrier-frequency wavelength. The polarization mismatch $X(\theta)$ can be regard as sinusoidal functions [23]. But the index of d is environment-dependent. It equals to 4 in free space. We should fix the index in real environment.

To fit the index, we should know at least two different RSSI values at two different positions. In a period of time, a fixed position corresponds to a fixed phase. As we mentioned in Section 2 that one phase value corresponds two symmetrical positions on the track. Due to the distance difference, the RSSI values of these two locations will be different. As Fig. 12 shows, p_1 and p_2 have the biggest RSSI difference. Then we can use these two RSSI values and the diameter of the rotation track to fit the index.

4.2 Noise Measurement and Processing

The noise level has great influence on the distribution of phase difference. Under the same condition, the larger the noise is, the greater the range of the phase difference is. So it is not reliable if we always use the same P_{output} and transition probability. Therefore we try to extract noise information from the readings. Then, we can get a more accurate distribution of the phase difference by adding the variance to the original distribution.

The phase readings, however, are highly dynamic, which means we can not extract the noise directly. We assume that the phase noise and RSSI noise have similar order of magnitude. Then we use the same factor d that influences both RSSI and phase to estimate the phase noise. As a result, we choose to estimate the RSSI noise first, and then convert it to phase noise through the Eq. (11) and the relationship between distance d and phase θ [20] in the far-field

$$\theta = \left(\frac{2\pi}{\lambda} \times 2d + c\right) \bmod 2\pi, \tag{12}$$

where λ is the wavelength, and c is diversity term related to the hardware characteristics. And in the near-field, the phase can be estimated from the electric fields $\mathbf{E}$ [25]

$$E = j\eta \frac{kI_0 l_t}{2\pi d^2}\left[1 + \frac{1}{jkd} - \frac{1}{(kd)^2}\right] e^{-jkd}, \tag{13}$$

where k is the wavenumber, I_0 and l_t is the antenna's current and length, η is the intrinsic impedance of free space.

Actually, RSSI noise is the variation of RSSI corresponding to a fixed position. As we mentioned above, due to the distance difference, the RSSI values of two symmetrical positions on the track will have difference, while the phase values are same. Nevertheless, during the rotation, there must be a phase value whose corresponding positions have the same distance to the antenna. In Fig. 12, they are p_3 and

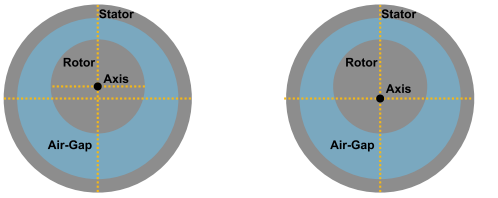

(a) The static eccentricity (b) The dynamic eccentricity

Fig. 13. The sketch of static and dynamic eccentricity.

p_4. Then this RSSI range is the RSSI noise. Therefore, we only need to find in the range of $[0, 2\pi]$, whose corresponding RSSI range is smallest.

4.3 The Effect of the Doppler Shift

When a signal source moves toward a certain direction at a constant rate, the wavelength and the frequency of the signal will change, leading to the Doppler shift. Such phenomenon becomes much more obvious when the moving speed of the signal source increase

$$f_{Doppler} = \frac{2f}{c}\vec{V}, \tag{14}$$

where f is the carrier frequency, $\vec{V}$ is the translation velocity, and c is the speed of the electromagnetic wave.

In addition to the constant Doppler frequency shift induced by the bulk motion of the target, there also exists micro-motion dynamics caused by rotation of the target. Specifically, the micro-motion dynamics will lead to Doppler modulations on the returned signal, which is called the micro-Doppler effect [26] as following:

$$f_{micro\_Doppler} = \frac{2f}{c}[\vec{\omega} \times \vec{r}], \tag{15}$$

where $\vec{\omega}$ is the rotation angular velocity, and $\vec{r}$ is the initial coordinates of the target in the antenna coordinates.

Specifically, high-speed rotation will lead to frequency shift, and therefore the reader cannot receive the backscattered signal at the original frequency. Moreover, the micro Doppler Effect is constantly changing as the tag rotates towards different orientation, which makes simple solutions such as compensating the frequency shift offline infeasible. However, we carry detailed theoretical calculation and simulations and the results show that given the condition that the distance between target and antenna is 10cm and the rotation speed is $10000RPM$ (which is very high), the frequency shift caused by Doppler Effect is only $31Hz/920MHz$, which can be negligible for the RFID sampling. This result also verify that our RFID-based design is robust in high-speed rotating scenario.

4.4 Different Direction of Eccentricity

In practice, a rotor's center axis may deviate toward various directions, and leading to different appearance of Int and Diff. For example, when the tag is approaching the antenna, Int will decrease and Diff will increase, and vice versa.

For simplicity, we classify eccentricity into two categories: approaching the antenna and deviating the antenna. To solve both of the two kinds of eccentricity, RED includes two detection modules. Specifically, RED first detects whether the received signal exhibits the feature of either type of eccentricity. If the signal's appearance fits any of these two types, RED will raise an alarm. Otherwise, RED considers the machinery is working properly. An extreme case is when the tag deviates far away from the antenna, the E-Points will rarely appear or even disappear. RED cannot make a judgement in this scenario. To tackle this problem, we set a timer T which records the time duration from the last appearance of E-Point to now. If T exceeds a threshold, eccentricity is considered has occurred.

4.5 Different Eccentricity Types

Fig. 13 shows the difference between static and dynamic eccentricity. In the static case, the rotation axis is the center of the rotor but the it has a shift from the center of the stator. In the dynamic case, the rotor also has a shift but the rotation axis remains as the center of the stator. It means that when dynamic eccentricity occurs, the rotation axis does not change but the outermost envelop of the rotor expands, which can be considered as the circular track of a dot (or the tag) on the rotor has a larger radius. However, the dynamic case can still be handled by our system.

From the analysis in above sections we can easily find the fact that the detection of RED only relies on those points closest to the antenna (E-points). In the static case, the closest points approach or deviate from the antenna along with the shift of the rotation axis. And in the dynamic case, if the normal line of the antenna is out of the circular track of the tag (this is a common case in our deployment since the tag is attached close to the rotation axis), the closest points approach the antenna while the radius increases.

We simulate the dynamic eccentricity by increasing the radius of tag's track and the CDF of Int and $Diff$ is shown in Fig. 7. The result shows that in terms of the signal characteristics captured by RED, the dynamic eccentricity is similar to the approaching case in the static eccentricity

5 Evaluation

5.1 Implementation

The devices we use are shown in Fig. 3. The RFID system operates at 920-926 MHz band. The tags adopt LLRP protocol [27], [28] to communicate with the reader. The mean sampling rate is 40 Hz [17]. To simulate the high speed rotating machinery, the centrifuge rotates at 10,000 RPM.

5.2 Methodology

We mainly use three metrics to evaluate the performance of RED: *True Positive Rate (TPR)*, *False Positive Rate (FPR)*, and *Latency*. TPR represents the percentage that RED correctly detects eccentricity. FPR represents the percentage that RED detects falsely when there is no eccentricity. Latency represents how long it takes for RED to detect the eccentricity.

We mainly adjust following settings:

- *Shift distance (Δd).* Shift distance represents the smallest shift we should detect. Every time we move the centrifuge by the same distance, and then evaluate the performance.

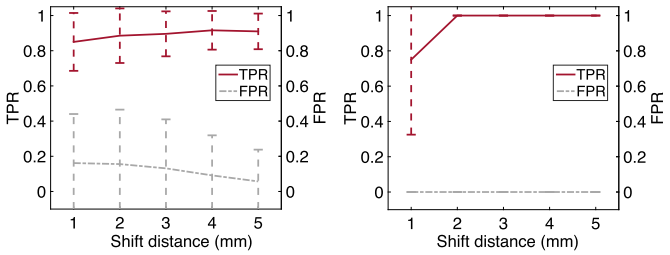

(a) The result when the tag approaches the antenna

(b) The result when the tag deviates from the antenna

Fig. 14. The average and variance of TPR and FPR with different shift distances when $d = 6\text{cm}$.

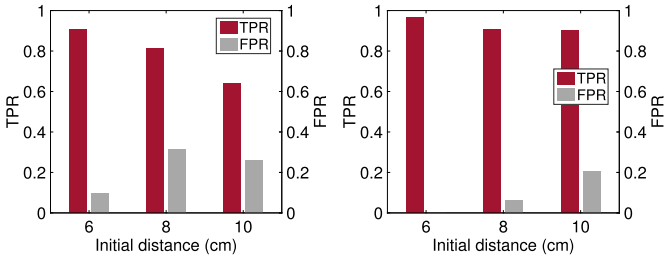

(a) The result when the tag approaches the antenna

(b) The result when the tag deviates from the antenna

Fig. 15. The TPR and FPR over different initial distances when $\Delta d = 7\text{mm}$.

- *Initial distance (d).* Initial distance means the distance between the tag and the antenna when we deploy RED.
- *Noise (n).* We conduct experiments in noisy environments, and try to evaluate the effect of the noise processing module.

In the training phase, we collect data for 1 minute at the initial position. In the testing phase, we move the tag in two directions, approaching and deviating the antenna. At each position, we collect data for 5 seconds and repeat 10 times.

5.3 Accuracy of RED

To evaluate accuracy of RED, we place the centrifuge 6 cm away from the antenna, and change Δd from 1 to 7 mm. The results are shown in Fig. 14. The overall TPR is 93.6 percent, while the FPR is 4.9 percent. For the approaching case, The overall TPR can reach 90.8 percent, while FPR is 9.8 percent. When Δd is set to 1 mm, the average of TPR is 85 percent and the FPR is 16 percent. As Δd increases, the TPR rises and the FPR falls. That's because the difference between the RSSI and phase readings before and after eccentricity is more obvious when Δd is larger. When the tag deviates, the performance of RED is better than the approaching case. The reason is that when the tag deviates from the antenna, the number of E-points will decrease. If there is no E-points in a rotation period, Int will significantly increase, which is easy to be detected by the HMM.

5.4 Impact of Different Initial Distance

We choose three different initial distances, while Δd is 7 mm. The results are shown in Fig. 15. Whether the tag is approaching or deviating from the antenna, the results are similar. As d increases, the TPR decreases and the FPR increases. The reason is that according to the wireless signal model, when initial distance increases, the signal strength is weaker and the same shift will cause smaller signal change (especially in mm-level), which is harder to detect. If it is allowed to enhance the strength of the source signal, our system can work with a larger distance.

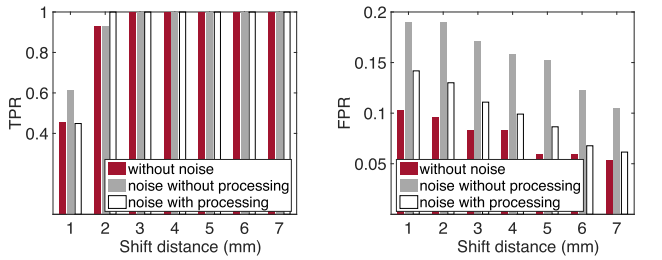

(a) The TPR over different shift distances

(b) The FPR over different shift distances

Fig. 16. The Impact of noise when $d = 8\text{cm}$.

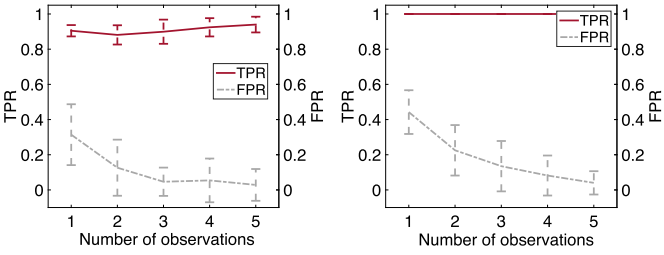

(a) The result when the tag approaches the antenna

(b) The result when the tag deviates from the antenna

Fig. 17. The average and variance of TPR and FPR over different numbers of observations when $d = 6\text{cm}$, $\Delta d = 7\text{mm}$.

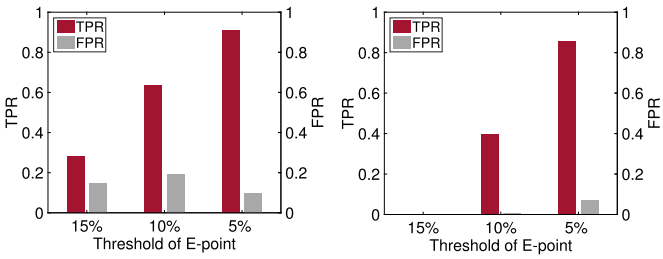

(a) The result when the tag approaches the antenna

(b) The result when the tag deviates from the antenna

Fig. 18. The overall TPR and FPR over different thresholds of E-point.

5.5 Impact of Noise

Red has the ability to tolerate noise, and we try to evaluate the effect of noise processing. When $d = 8\text{cm}$ and the tag deviates from the antenna, we collect data in both clean and noisy (a person is walking around) environments, and we enable or disable the noise processing module. From Fig. 16 we can see that when the environment is noisy, FPR increases. After noise processing, the FPR returns to the normal level. This result demonstrates that the noise processing module is effective.

5.6 Impact of the Number of Observations

The number of observations of RED is a key metric. It not only affect the accuracy, but also is related to the latency of RED. The more samples we observe, the latency is longer. The impact of changing the number of observations is shown in Fig. 17. As we observe more samples, the performance getting

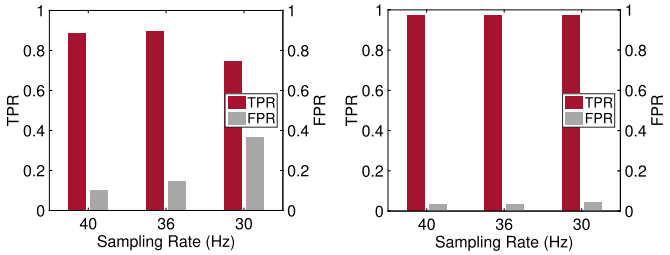

(a) The result when the tag approaches the antenna

(b) The result when the tag deviates from the antenna

Fig. 19. The overall TPR and FPR over different sampling rates when $d = 6\text{cm}$.

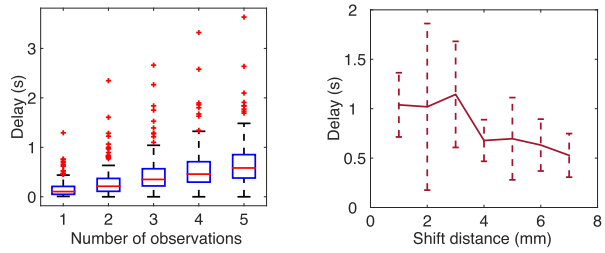

(a) The result when Δd ranging from 1 to 7 mm

(b) The result when the tag approaches the antenna

Fig. 20. The latency when $d = 6\text{cm}$.

better in both cases. So there is a trade off between latency and accuracy. We will discuss about this in a later subsection.

5.7 Impact of E-Point Threshold

We conduct experiments to examine the impact of choosing E-points. Fig. 18 shows the result. We can see that when the threshold of E-point is higher, the TPR and the FPR are better. The reason is that the difference is more significant around the maximum. The farther from the maximum, the expected $Diff$ is larger and the expected Int is smaller. The influence of eccentricity is less. So we choose 5 percent as the threshold of E-point.

5.8 Impact of Sampling Rate

Sampling rate is also an important factor which affects the performance of RED. As shown in Fig. 19, the TPR decreases and the FPR increases with the decrease of the sampling rate. The reason is low sampling rate leads to the inaccurate training model, which further leads to unreliable detection result. What's worse, lower sampling rate also increases the detection latency. Considering that eccentricity should be detected timely, the sampling rate should be sufficiently high to ensure low detection latency. The lower bound of sampling rate depends on the latency requirement. We also evaluate the effect of fixing environment-dependent factors module. The results are shown in Table 2. We can see that this module brings improvement in the accuracy.

5.9 Detection Latency

In the industrial scenarios, it is very dangerous if a rotation machine runs under eccentricity for too long or very likely it will cause serious accident. Therefore, the detection latency is an important factor to consider in our design. To get the CDF shown in Fig. 7, the sampling time is typical several minutes according to our study which is unacceptable for a detection system. The RUM model we propose can detect the eccentricity within 1 second, which can allow the control system to take actions in a timely manner, while a similar wireless detection system requires a signal segment of at least 4 seconds[11]. We set d at 6 cm, and adjust the shift distance and the number of observations. Fig. 20a shows the distribution of latency over different numbers of observations, while Δd ranges from 1 to 7 mm. We can see that when the number of observations is small, although the accuracy is low, the latency is low. It can reach $0.1615s$ when the number of observations is 1. But low accuracy means more unnecessary downtime of the machinery. The economic loss brings by low accuracy is unacceptable. So we think observing 4 samples is proper.

The distance between the tag and antenna also affects the latency. As Fig. 20b shows, as the tag approaches the antenna, the latency decreases. The reason is that the number of E-points reduces, so the expected Int increases.

TABLE 2
The Effect of Fixing Environment Factors

	Approaching		Deviating	
	With	Without	With	Without
TPR	0.906	0.891	0.832	0.830
FPR	0.103	0.112	0.114	0.119

6 Related Works

In this section, we briefly review the related works, by classifying them into two main categories.

Eccentricity Detection of Rotating Machinery. Different methods have been developed for rotating machinery's eccentricity detection. Various fault symptoms are used in the detection method, including vibration signals [3], thermal features [4], acoustic signals [5], oil debris [6], and so on. These symptoms can reflect the state of machinery, but they have their own limitations. To measure vibration signals and thermal signals, special sensors should be embedded into the machinery. Measuring acoustic signals and oil debris are via the non-intrusive method. However, it requires a complete system to measure oil debris, which is complex and expensive. Acoustic signals should be measured in a quiet environment. RFID-based system is non-intrusive and low-cost. It's easy to deploy in various environment.

RFID-Based Sensing. RFID-based sensing has been developed for several years. The researches are aimed at measuring different physical properties, and the common ground of them is to find how these properties affect the RSSI signal, then extract information from the received signals. Bhattacharyya *et al.* [29] leverage RFID infrastructures to design a wireless temperature sensor by using the changes in tag power characteristics. Manzari *et al.* [16] explore the possibility to integrate chemical species into an RFID tag, and then improve the sensing ability of tag. Tagbeat [17] quantifies the change in phase corresponding to the track of rotation. By recovering the periodic changes in phase, it can measure the vibration period of the device. RIO [19] is based on the impedance changing when a human finger touches a tag. The impedance change influence the phase readings,

which makes RFID-based touch sensing possible. Twins [18] leverages the interference among passive tags to do motion detection and achieve high precision.

The tag's orientation is also an interesting factor to study. RF-Compass [12] navigates the robot by using the RFID signals to partition the space based on the robot's consecutive moves. Griffin *et al.* [23] quantify the basic relationship between multiple factors and the RSSI, including the polarization factor. Tagyro [13] finds that polarization leads to the inaccurate readings, so designs a recovery algorithm to make the measurement reliable. PolarDraw [14] leverages the relationship between the RSSI readings and the angle of the tag to track the handwriting on the board.

The researches above can all provide a high precision result in the case of stationary or low-speed moving tags. Our goal is to offer further insight into the signal change regularities in the high-speed rotation scenario, and leverage them to achieve high precision and low latency detection.

7 Conclusion

RFID-based sensing, namely to sense physical phenomenon according to the RFID signals, is deemed as a promising technique in the area of cyber-physical systems. In this paper, we advance the state of the arts, by tackling the problem of RFID-based eccentricity detection for high-speed rotating machinery. This problem has great significance in industry, while producing non-trivial challenges in applying RFID-based sensing techniques. Our proposal called RED, utilizes the temporal and phase distributions of tag readings as effective features for eccentricity detection. Implementation of RED offers a non-intrusive, low-cost, and real-time solution, which is applicable to all kinds of rotating machinery.

There are also some limitations or future works can be discussed about our system. One of those is the cost of RFID readers. Although tags are cheap enough, each reader usually costs $600. However, in typical application scenarios, very often there are multiple machineries working in the same space. We dont need to deploy a separate reader for every monitored target. Monitoring multiple targets can indeed share the capacity of one reader. Therefore, our solution in practice is to deploy one reader and multiple antennas. The reader and the antennas at different locations are connected via feeder cables. The cost of a reader is relatively high but amortized. The cost of the feeder cable and the antenna is very low. Another issue is to determine the exact eccentric displacement, rather than treat the eccentricity as a binary event. As far as we know, this problem is very hard to address using the RFID technology, due to the limited phase resolution of RFID signals. We deem mm-wave radar an alternative solution.

Acknowledgments

This work was supported by the National Key R&D Program of China 2017YFB1003000, the NSFC No. 61772306, No. 61672320, and No. 61902213, the NSFC Key Project No. 61632008, and the NSF Grant CNS-1837146.

References

[1] Y. Lei, Z. He, and Y. Zi, "Application of an intelligent classification method to mechanical fault diagnosis," *Expert Syst. Appl.*, vol. 36, no. 6, pp. 9941–9948, 2009.

[2] T. Loutas, D. Roulias, E. Pauly, and V. Kostopoulos, "The combined use of vibration, acoustic emission and oil debris on-line monitoring towards a more effective condition monitoring of rotating machinery," *Mech. Syst. Signal Process.*, vol. 25, no. 4, pp. 1339–1352, 2011.

[3] C. Li, R.-V. Sánchez, G. Zurita, M. Cerrada, and D. Cabrera, "Fault diagnosis for rotating machinery using vibration measurement deep statistical feature learning," *Sensors*, vol. 16, no. 6, pp. 895–913, 2016.

[4] W.-K. Wong, C.-K. Loo, W.-S. Lim, and P.-N. Tan, "Thermal condition monitoring system using log-polar mapping, quaternion correlation and max-product fuzzy neural network classification," *Neurocomputing*, vol. 74, no. 1, pp. 164–177, 2010.

[5] V. Arumugam, A. A. P. Sidharth, and C. Santulli, "Failure modes characterization of impacted carbon fibre reinforced plastics laminates under compression loading using acoustic emission," *J. Composite Materials*, vol. 48, no. 28, pp. 3457–3468, 2014.

[6] C. Li, J. Peng, and M. Liang, "Enhancement of the wear particle monitoring capability of oil debris sensors using a maximal overlap discrete wavelet transform with optimal decomposition depth," *Sensors*, vol. 14, no. 4, pp. 6207–6228, 2014.

[7] T. M. Wolbank and P. E. Macheiner, "Adjustment, measurement and on-line detection of air gap asymmetry in AC machines," in *Proc. Eur. Conf. Power Electron. Appl.*, 2007, pp. 1–8.

[8] S. B. Chaudhury, M. Sengupta, and K. Mukherjee, "Vibration monitoring of rotating machines using MEMS accelerometer," *Int. J. Scientific Eng. Res.*, vol. 2, no. 9, pp. 5–11, 2014.

[9] A. Brkovic, D. Gajic, J. Gligorijevic, I. Savic-Gajic, O. Georgieva, and S. Di Gennaro, "Early fault detection and diagnosis in bearings for more efficient operation of rotating machinery," *Energy*, vol. 136, pp. 63–71, 2017.

[10] Y. Wei, Y. Li, M. Xu, and W. Huang, "A review of early fault diagnosis approaches and their applications in rotating machinery," *Entropy*, vol. 21, no. 4, 2019, Art. no. 409.

[11] E. T. Esfahani, S. Wang, and V. Sundararajan, "Multisensor wireless system for eccentricity and bearing fault detection in induction motors," *IEEE/ASME Trans. Mechatronics*, vol. 19, no. 3, pp. 818–826, Jun. 2014.

[12] J. Wang, F. Adib, R. Knepper, D. Katabi, and D. Rus, "RF-compass: Robot object manipulation using RFIDs," in *Proc. 19th Annu. Int. Conf. Mobile Comput. Netw.*, 2013, pp. 3–14.

[13] T. Wei and X. Zhang, "Gyro in the air: Tracking 3D orientation of batteryless Internet-of-Things," in *Proc. 22nd Annu. Int. Conf. Mobile Comput. Netw.*, 2016, pp. 55–68.

[14] L. Shangguan and K. Jamieson, "Leveraging electromagnetic polarization in a two-antenna whiteboard in the air," in *Proc. 12th Int. Conf. Emerging Netw. EXperiments Technol.*, 2016, pp. 443–456.

[15] J. Liu, M. Chen, S. Chen, Q. Pan, and L. Chen, "Tag-compass: Determining the spatial direction of an object with small dimensions," in *Proc. IEEE Conf. Comput. Commun.*, 2017, pp. 1–9.

[16] S. Manzari, C. Occhiuzzi, S. Nawale, A. Catini, C. Di Natale, and G. Marrocco, "Polymer-doped UHF RFID tag for wireless-sensing of humidity," in *Proc. IEEE Int. Conf. RFID*, 2012, pp. 124–129.

[17] L. Yang, Y. Li, Q. Lin, X.-Y. Li, and Y. Liu, "Making sense of mechanical vibration period with sub-millisecond accuracy using backscatter signals," in *Proc. 22nd Annu. Int. Conf. Mobile Comput. Netw.*, 2016, pp. 16–28.

[18] J. Han *et al.*, "Twins: Device-free object tracking using passive tags," *IEEE/ACM Trans. Netw.*, vol. 24, no. 3, pp. 1605–1617, Jun. 2016.

[19] S. Pradhan, E. Chai, K. Sundaresan, L. Qiu, M. A. Khojastepour, and S. Rangarajan, "RIO: A pervasive RFID-based touch gesture interface," in *Proc. 23rd Annu. Int. Conf. Mobile Comput. Netw.*, 2017, pp. 261–274.

[20] ImpinJ, "Application Note-Low Level User Data Support," 2019. [Online]. Available: https://support.impinj.com/hc/en-us/articles/202755318-Application-Note-Low-Level-User-Data-Support

[21] A. Polat, Y. Ertuğrul, and L. Ergene, "Static, dynamic and mixed eccentricity of induction motor," in *Proc. IEEE 10th Int. Symp. Diagnostics Elect. Machines Power Electron. Drives*, 2015, pp. 284–288.

[22] Alien Technology, "Alien 'G' Inlay," 2019. [Online]. Available: http://www.alientechnology.com

[23] J. D. Griffin and G. D. Durgin, "Complete link budgets for backscatter-radio and RFID systems," *IEEE Antennas Propag. Mag.*, vol. 51, no. 2, pp. 11–25, Apr. 2009.

[24] H. T. Friis, "A note on a simple transmission formula," *Proc. IRE*, vol. 34, no. 5, pp. 254–256, 1946.

[25] C. A. Balanis, *Antenna Theory: Analysis and Design*. Hoboken, NJ, USA: Wiley, 2016.
[26] V. C. Chen, F. Li, S. S. Ho, and H. Wechsler, "Micro-doppler effect in radar: Phenomenon, model, and simulation study," *IEEE Trans. Aerosp. Electron. Syst.*, vol. 42, no. 1, pp. 2–21, Jan. 2006.
[27] LLRP toolkit, 2019. [Online]. Available: http://www.llrp.org
[28] J. Han *et al.*, "GenePrint: Generic and accurate physical-layer identification for UHF RFID tags," *IEEE/ACM Trans. Netw.*, vol. 24, no. 2, pp. 846–858, Apr. 2016.
[29] R. Bhattacharyya, C. Floerkemeier, S. Sarma, and D. Deavours, "RFID tag antenna based temperature sensing in the frequency domain," in *Proc. IEEE Int. Conf. RFID*, 2011, pp. 70–77.

Yuan He received the BE degree from the University of Science and Technology of China, Hefei, China, the ME degree from the Institute of Software, Chinese Academy of Sciences, Beijing, China, and the PhD degree from the Hong Kong University of Science and Technology, Hong Kong. He is currently an associate professor with the School of Software and BNRist of Tsinghua University, Beijing, China. His research interests include wireless networks, Internet of Things, pervasive and mobile computing. He is a senior member of the IEEE and member of the ACM.

Yilun Zheng received the BS degree in electronic engineering from Tsinghua University, Beijing, China, in 2015, and the MS degree from Tsinghua University, Beijing, China, in 2018. Her research interests include the field of low power wireless communication. She is a student member of the IEEE.

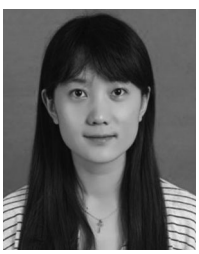

Meng Jin received the BS, MS, and PhD degrees in computer science from Northwest University, Kirkland, Washington, in 2012, 2015, and 2018, respectively. She is currently a postdoctoral researcher at the School of Software, Tsinghua University, Beijing, China. Her main research interests include backscatter communication, wireless network co-existence at 2.4 GHz and clock synchronization. She is a student member of the IEEE.

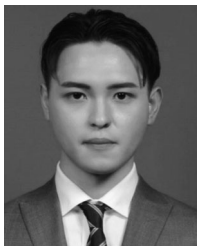

Songzhen Yang received the BS degree in the School of Software from Tsinghua University, Beijing, China, where he is currently working toward the MS degree. He currently works in the Systems and Ubiquitous Networking (SUN) Group in the Institute of Trustworthy Networks and Systems(TNS), advised by Yuan He. His research interests include backscatter communication and sensing. He is a student member of the IEEE.

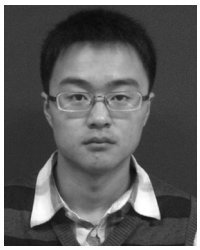

Xiaolong Zheng received the BE degree from the Dalian University of Technology, Dalian, China, in 2011, and the PhD degree from the Hong Kong University of Science and Technology, Hong Kong, in 2015. He was a postdoctoral researcher at Tsinghua University, Beijing, China, during 2015-2018 and is currently a research associate professor and PhD supervisor in the School of Computer Science, Beijing University of Posts and Telecommunications, Beijing, China. His research interests include wireless sensor networks and ubiquitous computing. He is a member of the IEEE and ACM.

Yunhao Liu received the BS degree in Automation Department from Tsinghua University, Beijing, China, and the MS and PhD degrees in computer science and engineering, Michigan State University, East Lansing, Michigan. He is currently MSU foundation professor and chairperson in Department of Computer Science and Engineering, Michigan State University, East Lansing, Michigan, and holds Chang Jiang chair professorship at Tsinghua University, Beijing, China. He is an ACM distinguished speaker and serves as the editor-in-chief of the *ACM Transactions on Sensor Networks*. His research interests include sensor network and pervasive computing, peer-to-peer computing, IoT and supply chain. He is a fellow of the IEEE and ACM.